Open Geospace General Circulation Model simulation of a substorm: Axial tail instability and ballooning mode preceding substorm onset

J. Raeder,[1] P. Zhu,[2] Y. Ge,[1] and G. Siscoe[3]

Received 29 June 2010; revised 7 October 2010; accepted 12 October 2010; published 31 December 2010.

[1] Recent global simulations of substorms show that before the onset of near-Earth reconnection the pressure equilibrium in the tail breaks down. This instability has no cross-tail variation and is thus not a ballooning mode, and it is also distinct from the tearing mode. Here, we analyze an Open Geospace General Circulation Model simulation run of the 23 March 2007 substorm and find the same instability. Because this mode has no significant cross-tail variation associated with it we call it the KY0 mode. Besides the KY0 mode we also find the classical ballooning mode in the simulation. It has a wavelength of ~0.5 R_E and is marginally, but sufficiently, resolved as shown by a higher-resolution control run. These results suggest a new scenario for the substorm expansion phase onset. During the growth phase magnetic flux is added to the lobes and the plasma sheet thins but remains in equilibrium. When force balance is no longer possible the KY0 instability grows and accelerates plasma tailward. The divergence of the resulting tailward flow reduces the normal magnetic field and thereby makes the current sheet tearing unstable. The tearing mode grows right out of the KY0 mode. The classical ballooning mode grows at the same time and is superimposed on the KY0 mode, but its role in initiating reconnection is still unclear. The growth time of the KY0 mode, ~2 min, is both consistent with the notion of an explosive growth phase and with recent ground-based observation of the initial growth of auroral arcs before auroral breakup.

Citation: Raeder, J., P. Zhu, Y. Ge, and G. Siscoe (2010), Open Geospace General Circulation Model simulation of a substorm: Axial tail instability and ballooning mode preceding substorm onset, *J. Geophys. Res.*, *115*, A00I16, doi:10.1029/2010JA015876.

1. Introduction

[2] It is generally accepted that magnetic reconnection is the main mechanism that dissipates power during a substorm. It is less clear, however, whether the beginning of magnetic reconnection in the magnetotail also signifies the onset of the substorm expansion phase itself (i.e., the "outside in" scenario [see, e.g., *Baker et al.*, 1996, 1999; *Sibeck and Angelopoulos*, 2008; *Angelopoulos et al.*, 2008a, 2008b]), or if a different process happens closer to Earth that triggers the reconnection onset in the magnetotail (i.e., the "inside out" scenario [*Roux et al.*, 1991; *Lui et al.*, 1992, 2007; *Pu et al.*, 2001]. The physics of the substorm expansion phase onset is very difficult to disentangle because many different phenomena occur within a few minutes of substorm expansion phase onset. Many studies have focused on ordering these phenomena, such as the initial auroral brightening, the beginning of magnetic bays, Pi2 pulsations, fast plasma sheet flows, injection of energetic particles, and dipolarization of the near Earth magnetic field (also called current disruption) [see, e.g., *Liou et al.*, 2002; *Kepko et al.*, 2004; *Rae et al.*, 2009; *Angelopoulos et al.*, 2008b; *Gabrielse et al.*, 2009, and references therein]. These efforts have been somewhat futile since the results of different studies often contradict each other and even the same data sets are interpreted quite differently by different authors, for example the recent observation of the 26 February 2008 event [*Angelopoulos et al.*, 2008b, 2009; *Lui*, 2009].

[3] It is generally accepted that the poor sampling of the magnetotail during substorms has been a main obstacle in resolving these contradictions. Although the THEMIS mission, the space probes and the extensive network of ground-based stations, is a tremendous step forward, the coverage in the tail can at best resolve radial dependencies, while there is virtually no resolution in local time by the five probes. Thus, features that propagate azimuthally may be seen as propagating in-out, or out-in, depending on how they are inclined to the axis of observation. Although the ground-based capabilities have also increased dramatically [*Mende et al.*, 2009], and the ground-based instruments provide good coverage in local time, mapping ionospheric features to the tail

[1]Space Science Center and Physics Department, University of New Hampshire, Durham, New Hampshire, USA.
[2]Department of Engineering Physics and Department of Physics, University of Wisconsin-Madison, Madison, Wisconsin, USA.
[3]Center for Space Physics, Boston University, Boston, Massachusetts, USA.

0148-0227/10/2010JA015876

depends on magnetic field models and is thus afflicted with uncertainties.

[4] In order to fill the observational gaps global simulations of the magnetosphere have been used, with mixed success, to model substorms [see, e.g., *Lyon et al.*, 1981; *Slinker et al.*, 1995; *Raeder and Maynard*, 2001; *Raeder et al.*, 2001a, 2008; *Kuznetsova et al.*, 2007]. Since the global models are based on a fluid description they cannot include all the physical processes that occur during substorms. For example, particle injections into the inner magnetosphere are not included in the models. However, several models have at least been able to reproduce the basic loading-unloading cycle of substorms [*Raeder*, 1995; *Pulkkinen et al.*, 1998; *Raeder and McPherron*, 1998; *Elsen et al.*, 1998; *Wiltberger et al.*, 2000; *Raeder et al.*, 2001a; *Kuznetsova et al.*, 2007]. In each of these simulation studies the substorm was associated with reconnection in the tail, and none of these studies identified any specific process that triggered reconnection in the tail. Thus, the results from global MHD simulations are generally consistent with the basic Near Earth Neutral Line (NENL) model of substorms that stipulates that the onset of fast reconnection, i.e., reconnection between lobe field lines, triggers the onset [*Russell and McPherron*, 1973; *Hones*, 1979; *McPherron*, 1991; *Baker et al.*, 1996, 1999]. It must be kept in mind, however, that the expansion phase onset is defined by the brightening of an auroral arc, which is a rather subtle feature. Although some of the models produce a proxy for the aurora, it is fairly difficult to determine the beginning of the brightening of an arc, or the beginning of a change of some other auroral feature in the model. This difficulty is compounded by the rather poor spatial resolution of the models, which translates also to poor temporal resolution. Thus, the models are afflicted by the same "2 min problem" as the observations, i.e., the inability to order the processes that occur within a minute or two of the onset. The temporal ordering of processes occurring in the models has therefore not even been attempted.

[5] In spite of these shortcomings, global models are useful to investigate the substorm process, in particular, because they are the only self-consistent models available, and because they have been shown to reproduce the fundamental mode of energy conversion during a substorm, as well as other features such as dipolarization fronts and the substorm current wedge. Under the hypothesis that the model produces the correct phenomena for the right reason, we can then use the model to analyze the forces that initiate the substorm. Such an analysis has recently been performed by *Siscoe et al.* [2009], who showed that in generic substorm simulations, using both the Open Geospace General Circulation Model (OpenGGCM) and the Block Adaptive-Tree Solar-wind Roe-type Upwind Scheme (BATSRUS) codes, a MHD instability occurs that precedes the onset of reconnection. In a somewhat different study, *Zhu et al.* [2009] has used an OpenGGCM substorm simulation to evaluate the stability of the ballooning mode in the tail during all substorm phases. That study found that the near Earth tail should be marginally unstable at certain times. In this study we continue this work. After briefly introducing the OpenGGCM and the 23 March 2007 substorm in sections 2 and 3, we show in section 4 that the type of instability found by *Siscoe et al.* [2009] operates during this substorm. Furthermore, we show that the classical ballooning instability occurs as well and that the characteristic spatial oscillations are marginally resolved by the code. In section 5 we summarize our results and conclude that the ideal-like MHD instabilities precede reconnection and are thus the trigger of expansion phase onset.

2. OpenGGCM Model

[6] The OpenGGCM is a global coupled model of Earth's magnetosphere, ionosphere, and thermosphere. The magnetosphere part solves the MHD equations as an initial boundary value problem. The MHD equations are solved to within ~3 R_E of Earth. The region within 3 R_E is treated as a magnetosphere-ionosphere (MI) coupling region where physical processes that couple the magnetosphere to the ionosphere-thermosphere system are parameterized using simple models and relationships. The ionosphere-thermosphere system is modeled using the NOAA CTIM (Coupled Thermosphere Ionosphere Model [*Fuller-Rowell et al.*, 1996; *Raeder et al.*, 2001b]). The OpenGGCM has been described with some detail [see, e.g., *Raeder et al.*, 2001a, 2008; *Raeder*, 2003]; we thus refer the reader to these papers. In particular, *Raeder et al.* [2008] also discusses a simulation of the same substorm that is further analyzed here.

3. The 23 March 2007 Substorm

[7] We chose the 23 March 2007 substorm for this study because it has already been investigated by several groups [*Angelopoulos et al.*, 2008a; *Runov et al.*, 2008; *Raeder et al.*, 2008; *Zhu et al.*, 2009], and because we had an OpenGGCM simulation of this substorm available [*Raeder et al.*, 2008]. In the latter paper we showed that the simulation reproduces the salient features of a substorm that can be expected from a fluid simulation, in particular the auroral brightening, the development of the westward traveling surge, fast flows in the tail, and the dipolarization of the magnetic field in the near Earth tail. Of course, there are kinetic features that cannot be modeled with a fluid code, such as particle injections and auroral kilometric radiation. However, with a recently developed new model, in which the OpenGGCM is coupled with Rice Convection Model, we were also able to produce electron and proton injections for the same event, which compared quite well with observations [*Hu et al.*, 2010]. In this paper we do therefore not address the validity of the simulation but rather investigate in detail the processes that occur just around the time of the onset of the expansion phase in the simulation.

4. Tail Dynamics

[8] It might be assumed that a global simulation that is driven with observed solar wind and interplanetary magnetic field (IMF) parameters as input, and that reproduces the main features of a substorm, should essentially solve the substorm problem. In reality, it is not that simple.

[9] No simulation can reproduce all substorm features exactly as they are observed. The model input is already poorly known because the solar wind and the interplanetary magnetic field are not measured where they impact Earth, but in general more than 200 R_E upstream and several tens of R_E from the sun-Earth line. Furthermore, because of computational constraints the model solves a simplified set of equations augmented with various parameterizations for processes that are poorly understood. The numerical treatment of the

equations then introduces further errors. In particular, numerical diffusion tends to smear out sharp features in the solution. One thus has to be content with reproducing the salient features of a substorm such as dipolarization and the westward traveling surge (WTS). If the key features of the substorm are reproduced, albeit possibly not quite in the right place, or at the right time, or with the right magnitude, one may have some confidence that the model also behaves so for the right reasons, i.e., in the case of a substorm, that the reasons for the substorm onset in the model correspond to those in reality. Finding the reasons for which the model behaves as it does is still difficult. The model produces substantial amounts of data and our ability to visualize these data and to comprehend their meaning is limited. This task is complicated by the fact that the simulation results are affected by numerical shortcomings such as limited resolution and numerical diffusion and thus warrants great care.

[10] We analyze here a simulation run of the 23 March 2007 substorm event. Results from that simulation have already been presented by *Raeder et al.* [2008]. In that paper it was established by model-data comparisons that the simulation indeed reproduces the salient features of the substorm such as the auroral brightening, the WTS, and dipolarization of the near Earth tail. In that paper we showed that the substorm in the simulation was driven by reconnection occurring at one or more reconnection lines in the near Earth tail, i.e., that the observed features such as the WTS and dipolarization were a direct consequence of reconnection. We did not comment, however, on the processes that were responsible for the initialization of new reconnection lines, and deferred that analysis to future work.

[11] In the mean time, *Siscoe et al.* [2009] have investigated the force balance along the tail axis around the time of substorm expansion phase onset in a simplified geometry using two different global models. The key result of this study is as follows: During the growth phase the axial forces $(\mathbf{j} \times \mathbf{B})_x$ and $(-\nabla p)_x$ are in near perfect balance. However, just before the onset of reconnection, both forces are greatly reduced in the region between $-16\ R_E$ and $-13\ R_E$, and the forces are out of balance such that the pressure force exceeds the magnetic force. Thus, there is a net tailward force in that region that accelerates plasma away from the Earth. However, neither force changes direction, i.e., the magnetic force is still Earthward, and the pressure force is still tailward. The fact that the net force is only tailward distinguishes it from the forces that are active during reconnection. In the case of reconnection, there would be a similar tailward net force tailward of the x line, however, with a tailward magnetic force. In addition, one would expect Earthward of the x line a force imbalance where the Earthward magnetic force exceeds the tailward pressure force. Since that was not observed in those simulations, the force imbalance could not have resulted from reconnection but must have come from an ideal-like MHD instability. Here, we draw a subtle distinction between ideal and ideal-like instabilities. An ideal instability is one that can be described by the ideal MHD equations, i.e., without diffusion terms, whereas an ideal-like instability does not change the field topology (like all ideal MHD instabilities), but may still include resistive effects. Thus, an ideal-like mode cannot be tearing or reconnection. The nature of this instability was not further investigated by *Siscoe et al.* [2009].

[12] Figure 1 shows more detailed results from the 23 March 2007 simulation published earlier. In particular, we focus on the region where reconnection eventually begins. Figure 1 shows color coded the x component of the force imbalance, $\tilde{F}_x = (\mathbf{j} \times \mathbf{B} - \nabla \mathbf{p})_x$, the x component of the plasma velocity, and the parallel electric field $E_\parallel = \mathbf{E} \cdot \mathbf{B}/B$ for 5 different times in the region $-21\ R_E \le X \le -7\ R_E$, $Y = 0$, and $-7\ R_E \le Z \le 7\ R_E$. Figure 1 (left) shows color coded the x component of the plasma velocity, Figure 1 (middle) shows the force imbalance, and Figure 1 (right) shows the magnitude of the parallel electric field.

[13] At 1029 UT (Figure 1a) there is no flow in the central plasma sheet whose speed exceeds the speed of the flows in the surrounding regions. The flow speeds are of the order of a few tens of km/s. However, Figure 1a (middle) shows at this time a net tailward force density in the region between $X = -12\ R_E$ and $X = -15\ R_E$, indicating that the plasma here is being accelerated tailward. Figure 1a (right) shows the parallel electric field magnitude $E_\parallel$. Due to numerical errors there is a finite $E_\parallel$ almost everywhere in the tail, and it is somewhat enhanced in the current sheets. However, the $E_\parallel$ values are significantly lower than those usually found near a reconnection site.

[14] At 1 min later, 1030 UT, and shown in Figure 1b, the net tailward force density has accelerated the plasma to values in excess of 100 km/s tailward. The tailward force imbalance, shown in Figure 1b (middle), is still present, and thus the plasma is still being accelerated. There is also very little change of $E_\parallel$. Because the acceleration is only tailward and because $E_\parallel$ is small, the plasma acceleration cannot be due to reconnection or the tearing mode. We also checked B_z in this region (not shown here, but evident in Figure 2 below) and found it to be of significant positive value everywhere, demonstrating that no x line has formed.

[15] At 1031 UT (Figure 1c) the tailward flow has significantly accelerated and reaches values of −250 km/s. There is also a hint of Earthward acceleration now, i.e., the flow speeds Earthward of $-12\ R_E$ start to increase, but do not exceed 100 km/s. There is also a significant Earthward force density imbalance Earthward of $-12\ R_E$, but still no significant increase of $E_\parallel$ at the flow bifurcation.

[16] Figure 1d shows the situation 2 min later. The tailward flows have further accelerated and now reach nearly −400 km/s, while the Earthward flows have only marginally become stronger. $E_\parallel$ at the flow bifurcation is still small.

[17] Figure 1e shows the parameters 3 minutes later, at 1036 UT. Now the tailward flows exceed 500 km/s in magnitude and the Earthward flows are also significantly stronger and approaching 200 km/s. There are strong tailward forces tailward of the flow bifurcation and Earthward forces Earthward of the flow bifurcation. Also, $E_\parallel$ now approaches 1 mV/m almost everywhere in the current sheet.

[18] The flow acceleration during the first four minutes is clearly not related to the tearing mode or due to an x line. Therefore it must be an ideal-like MHD instability, whose nature is yet to be determined. At later times, the signature of the flow, force density, and $E_\parallel$ changes and is consistent with the formation of an x line.

[19] Because the current sheet becomes very thin one has to wonder whether the simulation code resolves the sharply bent magnetic field properly. At its thinnest, the current sheet is only one grid cell thick and thus at the limit of the

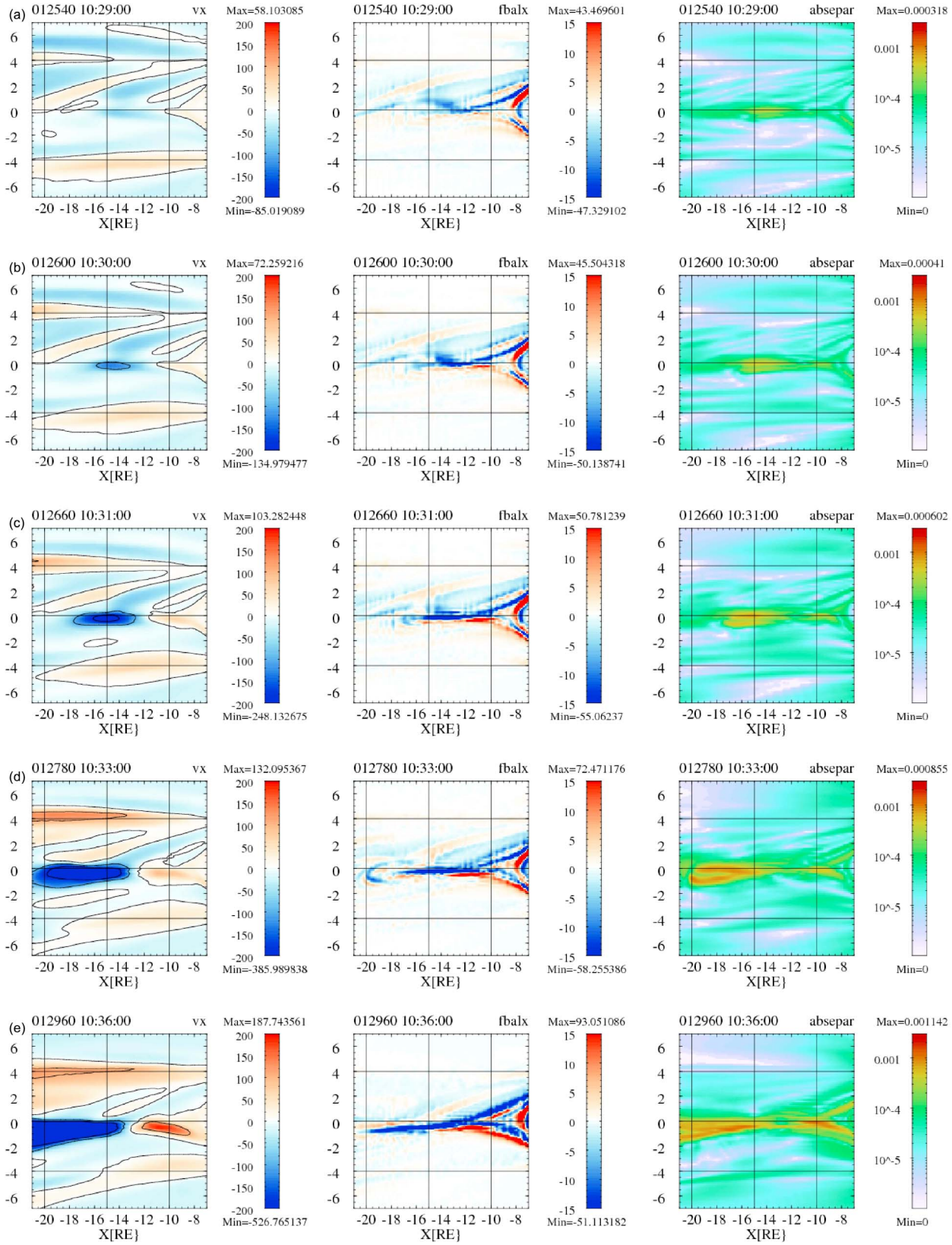

Figure 1. Cuts in the noon-midnight meridian, showing color-coded (left) plasma velocity x component (V_x) in km/s, (middle) force imbalance in the x direction in units of fN/m^3, and (right) magnitude of the parallel electric field in units of V/m. Figure 1 (left) also has contours at 50 km/s intervals. Different times, i.e., (a) 1029 UT, (b) 1030 UT, (c) 1031 UT, (d) 1033 UT, and (e) 1036 UT.

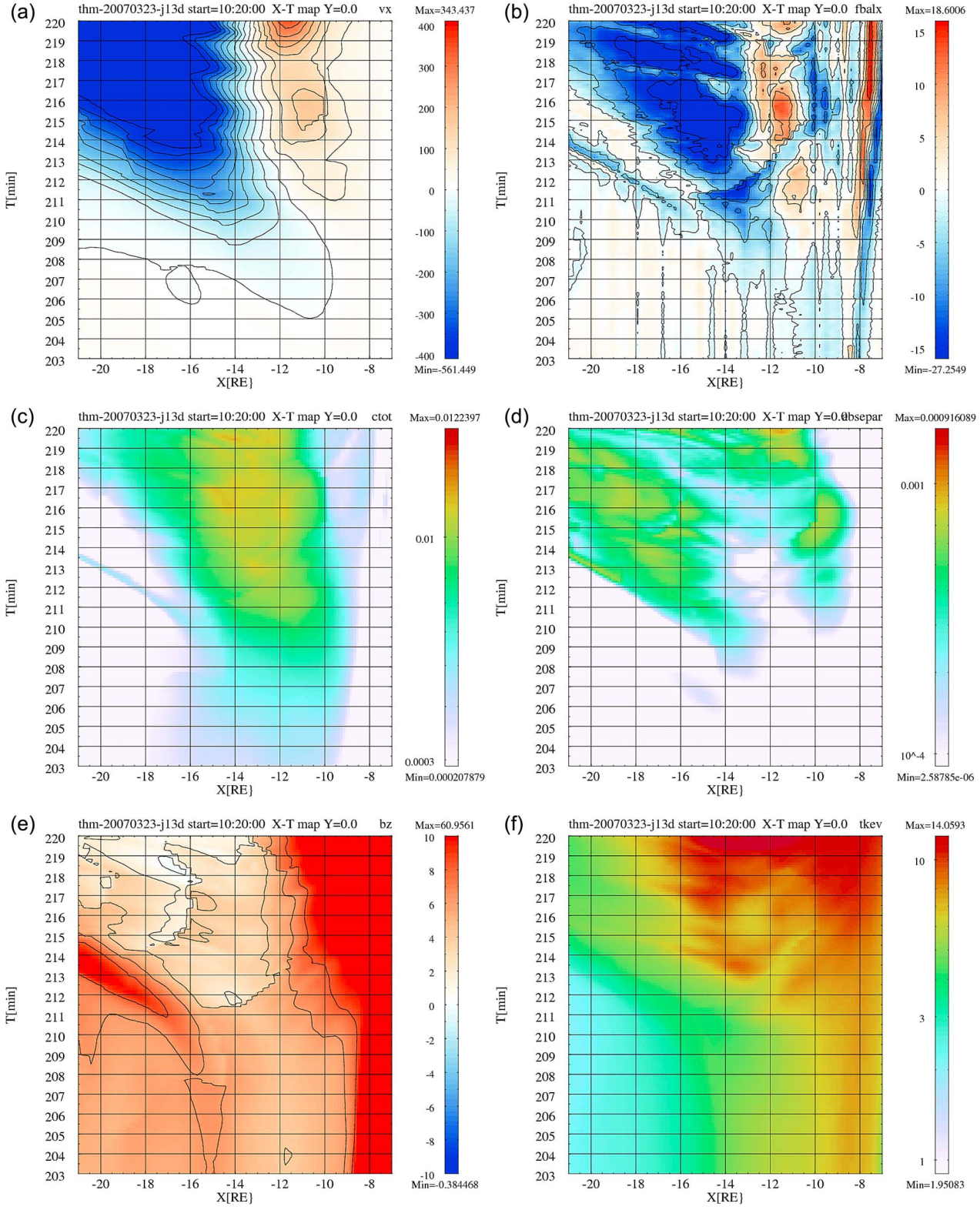

Figure 2. Space-time diagrams of several quantities in the tail along the line defined by Y = 0 and $B_x(Z) = 0$, i.e., along the noon-midnight meridian in the center of the current sheet. (a) The x component of the plasma velocity in km/s, (b) the x component of the force balance $\tilde{F}_x = (\mathbf{j} \times \mathbf{B} - \nabla \mathbf{p})_x$ in units of fN/m^3, (c) the magnitude of the current density in μA/m^2, (d) the magnitude of $E_{\|}$ in V/m, (e) the z component of the magnetic field in nT, and (f) the temperature in keV are shown. The vertical axis shows time in minutes since the start of the simulation run. For comparison with Figure 1, T = 210 min corresponds to 1030 UT. The horizontal axis is X_{GSE}, with the Earth to the right.

resolution. However, since the forces are all in the x direction we may ignore the y dependence, which should be weak, and average over the current sheet in the z direction. The force balance in the x direction, integrated over z, reads

$$\int_{z_1}^{z_2} \tilde{F}_x dz =$$

$$= \int_{z_1}^{z_2} (j_y B_z - j_z B_y) dz - \int_{z_1}^{z_2} \frac{\partial p}{\partial x} dz, \quad (1)$$

$$= \int_{z_1}^{z_2} \left(\frac{\partial B_x}{\partial z} - \frac{\partial B_z}{\partial x} \right) B_z dz - \int_{z_1}^{z_2} \frac{\partial p}{\partial x} dz, \quad (2)$$

$$\simeq B_z \int_{z_1}^{z_2} \frac{\partial B_x}{\partial z} dz - \int_{z_1}^{z_2} \frac{\partial p}{\partial x} dz, \quad (3)$$

$$= B_z (B_x(z_2) - B_x(z_1)) - \overline{P}_x, \quad (4)$$

where $\overline{P}_x$ represents the integrated $(\nabla p)_x$, and where we have made use of the assumptions that (1) there is no y dependence of any of the variables, (2) $B_y = 0$, (3) $B_z(x)$ varies slowly ($|\partial B_z/\partial x| \ll |\partial B_x/\partial z|$), and (4) B_z is constant as a function of z (if it were not, B_x would have to vary along x by the same amount because of $\nabla \cdot \mathbf{B} = \mathbf{0}$, but $B_x(x)$ varies only slowly), which are all reasonable assumptions for the tail current sheet. We now compare this to the numerical calculation. The pressure derivative is of no concern, because the pressure varies smoothly along x, and thus the derivative is calculated with high accuracy. However, the calculation of j_y involves differences of a rapidly varying function

$$j_y|_{i+1/2,j,k+1/2} =$$

$$= \left(\frac{\partial B_x}{\partial z} - \frac{\partial B_z}{\partial x} \right)|_{i+1/2,j,k+1/2}, \quad (5)$$

$$\simeq \frac{\partial B_x}{\partial z}|_{i+1/2,j,k+1/2}, \quad (6)$$

$$\simeq \left(B_{x,i+1/2,j,k+1} - B_{x,i+1/2,j,k} \right)/\Delta z, \quad (7)$$

where in equation (6) we used the same assumption as in equation (3), and equation (7) is the finite difference approximation of the derivative. Note that in the OpenGGCM MHD algorithm the magnetic field values are kept on the center of the cell faces (for example, B_x is located at $(i + 1/2, j, k)$), whereas the electric field and the current density are located at the center of the cell edges, for example, j_y is located at $(i + 1/2, j, k + 1/2)$ [*Raeder*, 2003; *Evans and Hawley*, 1988]. Here, i,j, and k are the indices corresponding to the cell centers.

[20] We now calculate the same integral as above over the current sheet. Because the function values are only available at discrete points we use the midpoint rule

$$\int_{z_1}^{z_2} f(z) dz = \Delta z \sum_{k=0}^{N} f\left(z_{k+1/2}\right) + O\left(\Delta z^2\right) \quad (8)$$

to evaluate the integral. This leads to

$$\int_{z_1}^{z_2} \tilde{F}_{x,\text{numerical}} dz =$$

$$\simeq B_z \Delta z \sum_{k=0}^{N} \left(B_{x,i+1/2,j,k+1} - B_{x,i+1/2,j,k} \right)/\Delta z - \overline{P}_x, \quad (9)$$

$$= B_z (B_x(z_2) - B_x(z_1)) - \overline{P}_x, \quad (10)$$

where the interval $[z_1, z_2]$ is partitioned into N grid cells with $z_2 = z_1 + (N + 1)\Delta z$. Thus, under the assumptions cited above, the numerical result (10) is the same as the analytical result (4). In particular, the accuracy of the force balance calculation in the code is independent of the curvature of the field, and thus there is no concern that the instability is caused by numerical inaccuracies.

[21] To explore the current sheet dynamics further, we employ the following technique. First, we determine the center of the current sheet by finding $B_x = 0$ for all X and the meridian Y = 0 for the entire time period of interest at specified intervals, in this case every 6 seconds, and for the spatial interval of interest, in this case $-21\ R_E \le X \le -7\ R_E$, as before. We then produce for every variable Φ of interest a map $\Phi(x, t, y = 0, z_0)$ with z_0 implicitly defined by $B_x(z_0) = 0$. These cuts are thus in the center of the current sheet and the midnight meridian. Such maps are similar to the keograms often used to display scanning photometer data in that they show a color coded value versus a time axis and a spatial axis.

[22] The variables velocity x component V_x, net force density x component $\tilde{F}_x$, magnitude of the current density $|\mathbf{j}|$, parallel electric field $E_{\|}$, magnetic field z component B_z, and temperature T are shown in Figure 2 in this projection. Time runs from bottom to top, and the Earth is to the right.

[23] At the beginning of the time period shown in Figure 2 there is a net tailward (negative) force density in the near Earth tail. At T = 206 min (corresponding to 1026 UT in the other plots) this region of net force shifts tailward and intensifies. From that time onward, until T = 211 min, the plasma in the region tailward of ~10 R_E is accelerated tailward. At T = 211 min the largest tailward velocity reaches ~250 km/s in magnitude, while there is no significant Earthward flow or acceleration. Figure 2c shows that the current density increases during this period in the same region. Since the total current is given by the difference of the magnetic fields in the southern and northern lobes, which changes little, the current sheet thins. Figure 2d shows that there is no significant parallel electric field during this interval, and thus reconnection is not taking place. Figure 2e shows a slight decrease of the normal component of the magnetic field, whose values are in the range of 4–6 nT. Figure 2d shows that there is no significant plasma heating during this time. This supports our previous conclusion that reconnection does not occur up to this time.

[24] At T~211 min several significant changes take place. First, while the tailward acceleration of the plasma tailward of ~12 R_E continues, there is now also a significant Earthward flow ≤50 km/s and accelerating. The peak current density increases further and saturates a few minutes later, but there is still no significant $E_{\|}$ until T~214 min. B_z rapidly decreases, and there is some plasma heating between T = 211 min and

T = 213 min, which significantly increases afterward. B_z decreases rapidly to values near zero. These features are consistent with a rapid collapse of the current sheet, while there are still no clear signs of tearing or reconnection visible. Specifically, at the location of the flow and force bifurcation, i.e., X = −13R_E, $E_{||}$ is virtually zero, and there is no significant Earthward force until T = 214 min. The heating may be real because of the intense current, but not related to reconnection. As we will argue below, reconnection begins after this period, and is characterized by much stronger plasma heating.

[25] At T~214 min another significant change takes place. There now appears a significant Earthward force at X~−12 R_E, which is part of a strong bifurcation, both in the forces and in the flow, at X~−12 R_E. Also, heating becomes intense and $E_{||}$ in the current sheet becomes larger. The normal magnetic field decreases to values below 2 nT. The peak current density saturates, but the region of peak current density still expands somewhat. Tailward flow speeds are in excess of 600 km/s magnitude. These signatures, taken together, clearly show that reconnection is taking place. The exact onset time and onset location of reconnection are difficult to determine. First, the numerical resolution is limited, and numerical diffusion tends to smear out features that should otherwise be sharp. However, the difficulty to pinpoint the exact reconnection onset may not entirely due to numerics. Comparing the reconnection signatures to the signatures at earlier times, when reconnection was clearly not present yet, one sees that the signatures are not all too different. In particular, the early ideal-like instability, as well as reconnection produce a divergence in the flow. While the ideal-like instability initially only produces tailward forces, we cannot be sure that it will also produce Earthward forces at a later stage, which may be indistinguishable from the Earthward forces that reconnection must produce. Plasma heating by itself is also not a unique reconnection feature because such heating may as well be adiabatic or ohmic dissipation in the current sheet. In the simulation, there is definitely some ohmic dissipation just because of numerical resistivity, which may or may not have a counterpart in nature. Finally, the presence of a parallel electric field is a necessary, but not a sufficient condition for reconnection [*Hesse et al.*, 2005]; however, in the simulation $E_{||}$ is possibly tainted by numerical diffusion.

[26] To summarize the results so far, we find the following scenario that ultimately leads to tail reconnection. First, the tail is slowly compressed during the growth phase, as dayside reconnection increases the flux in the tail lobes. During this compression phase, which may be partly or in its entirety the same as what is commonly known as the growth phase [*McPherron*, 1972; *Coroniti and Kennel*, 1972; *Sergeev et al.*, 1990], the current sheet thins slowly. Plasma and magnetic field is redistributed within the current sheet. However, the current sheet stays in equilibrium. The quasi-static evolution of the tail during the growth phase has been modeled extensively. For example, analytical Grad-Shafranov models exist [*Birn*, 1987; *Birn and Hesse*, 1992; *Birn and Schindler*, 2002], and numerical relaxation methods [*Hesse and Birn*, 1993; *Zaharia and Cheng*, 2003; *Lemon*, 2004] have been used to study them. These models have all in common that they eventually lead to some sort of catastrophe. In the case of analytic models, they become singular, and in the case of numerical models they become unstable. It is generally assumed that the magnetotail then enters a new evolutionary phase by starting reconnection. Our results indicate that the end of the growth phase is not necessarily signaled by the beginning of reconnection, but by the commencement of an ideal-like instability. The ideal MHD instabilities usually considered as candidates for the near-Earth tail are the ballooning instability [*Bhattacharjee et al.*, 1998] and the interchange instability [*Sonnerup and Laird*, 1963; *Sazykin et al.*, 2002]. Both of these instabilities are characterized by motion mainly in the x direction and rapid variations in the y direction. In case of the interchange instability, flux tubes of different entropy exchange places, which can lead to rapid flow and "plasma bubbles" [*Chen and Wolf*, 1993, 1999; *Birn et al.*, 2004]. For the ballooning instability one expects long finger-like structures that extend tailward, which have fairly small scale (a few 100 to a few 1000 km) in the y direction [*Lee and Wolf*, 1992; *Cheng and Zaharia*, 2004; *Zhu et al.*, 2004, 2007]. If either instability is present we should be able to identify it in the simulation in those places of the current sheet where the breakup eventually occurs.

[27] Figures 3 and 4 show several variables in the center of the current sheet as defined by $B_x = 0$, and as a function of X_{GSE} and Y_{GSE} at different times. Figure 3 (left) shows the plasma pressure, Figure 3 (middle) shows B_z, and Figure 3 (right) shows V_x. Time runs from top to bottom, and the times are the same as in Figure 1, i.e., 1029 UT, 1030 UT, 1031 UT, 1033 UT, and 1036 UT. Figure 4 employs the same format, except that Figure 4 (left) shows V_y, Figure 4 (middle) shows force balance in the y direction ($\tilde{F}_y = (\mathbf{j} \times \mathbf{B} - \nabla \mathbf{p})_y$), and Figure 4 (right) shows the force balance in the x direction, $\tilde{F}_x$.

[28] Neither Figure 3 nor Figure 4 show any sign of the interchange mode, although we have seen indications of interchange in other simulations [*Hu et al.*, 2010]. However, there are clear finger-like structures in all variables and at all times. The V_y plasma flow component (Figure 4, left) shows them most clearly. The fingers are already present at 1029 UT (Figure 4a), thus the ballooning mode has already been growing before the tailward flows were identified in the Y = 0 meridian. In fact, already accelerated tailward flows in the region of Y ≤ 0 correlate very well with the fingers seen in V_y, for example. The finger structures are visible in all variables shown here, although with different clarity.

[29] The lines in Figures 3 and 4 show the numerical grid. Specifically, the intersections of the lines are the cell centers. It is obvious that the finger structures are aligned with the grid lines. In addition, the oscillations in the y direction are mostly at the fundamental grid mode, i.e., peaks and troughs are on alternate grid lines. With such oscillations one has to be concerned that they could possibly be of numerical nature. However, numerical grid oscillations occur at unresolved discontinuities. In this case there is no discontinuity present that could possible be the cause of the oscillations. We thus conclude that the oscillations have a physical cause, and because of the characteristics of the perturbations, i.e., the alignment of pressure peaks with B_z peaks, we also conclude that this is the ballooning mode.

[30] The strict alignment of the waves with the grid and the dominance of the fundamental grid mode indicates that

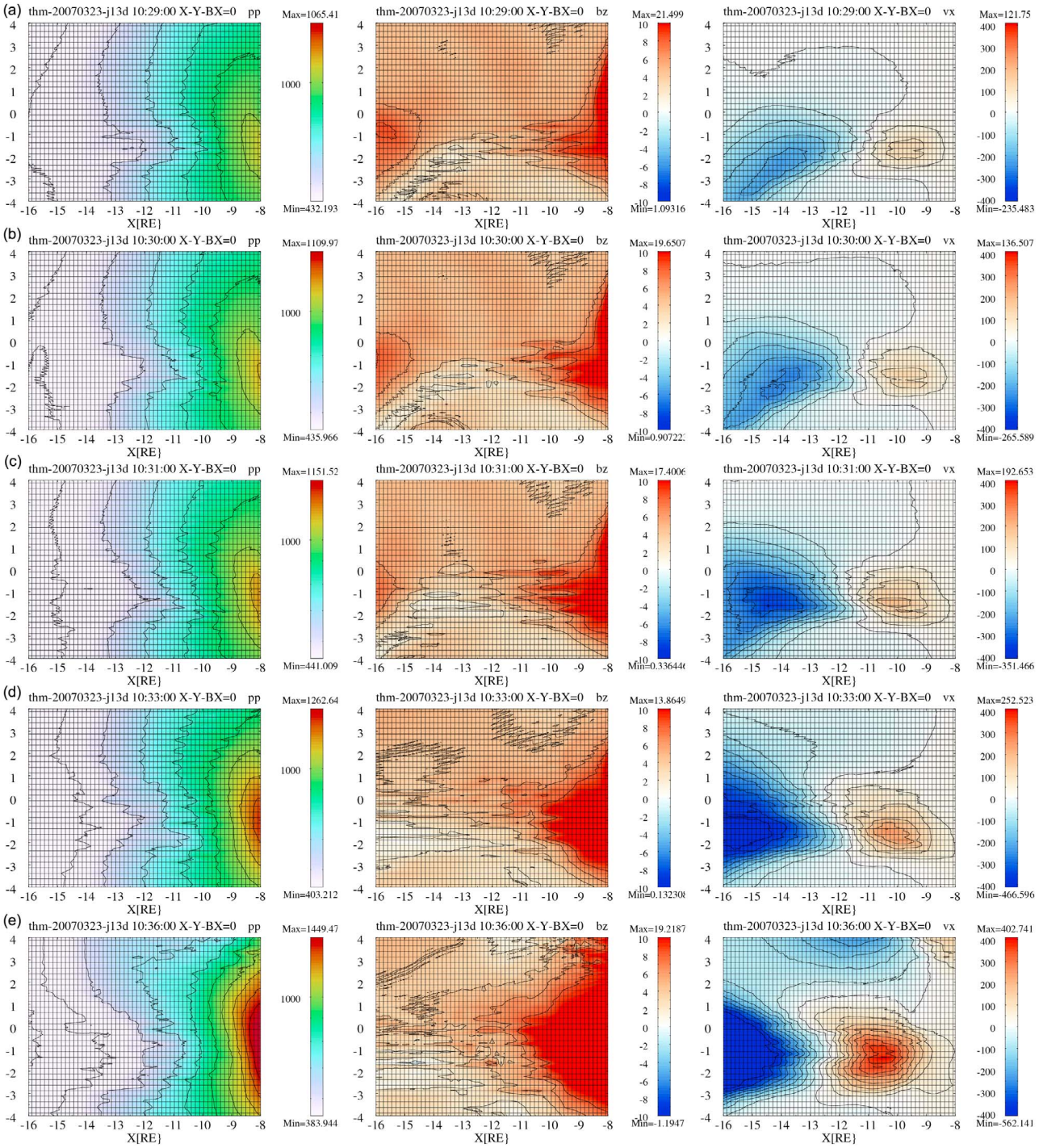

Figure 3. Variables in the center of the current sheet, as defined by $B_x = 0$ as a function of X_{GSE} and Y_{GSE}, and at different times. The (left) plasma pressure, (middle) B_z, and (right) V_x are shown. Times are the same as in Figure 1, i.e., (a) 1029 UT, (b) 1030 UT, (c) 1031 UT, (d) 1033 UT, and (e) 1036 UT.

the instability is likely under resolved. In a higher-resolved simulation, or in the limit of perfect resolution the mode would possibly grow at a shorter wavelength, but since the grid Nyquist frequency limits k_y space, the instability grows at the most unstable mode that the grid permits, which is the fundamental grid mode. Below, we will show a simulation result with higher resolution which demonstrates that the mode seen in Figures 3 and 4 is marginally resolved, i.e., that higher resolution does not lead to substantially larger k_y.

[31] The time evolution of the x component of the velocity is generally not consistent with the ballooning mode. In a pure ballooning mode there should be finger-like structures in V_x of alternating tailward and Earthward flows [*Ohtani and Tamao*, 1993; *Zhu et al.*, 2004]. Instead, Figure 3

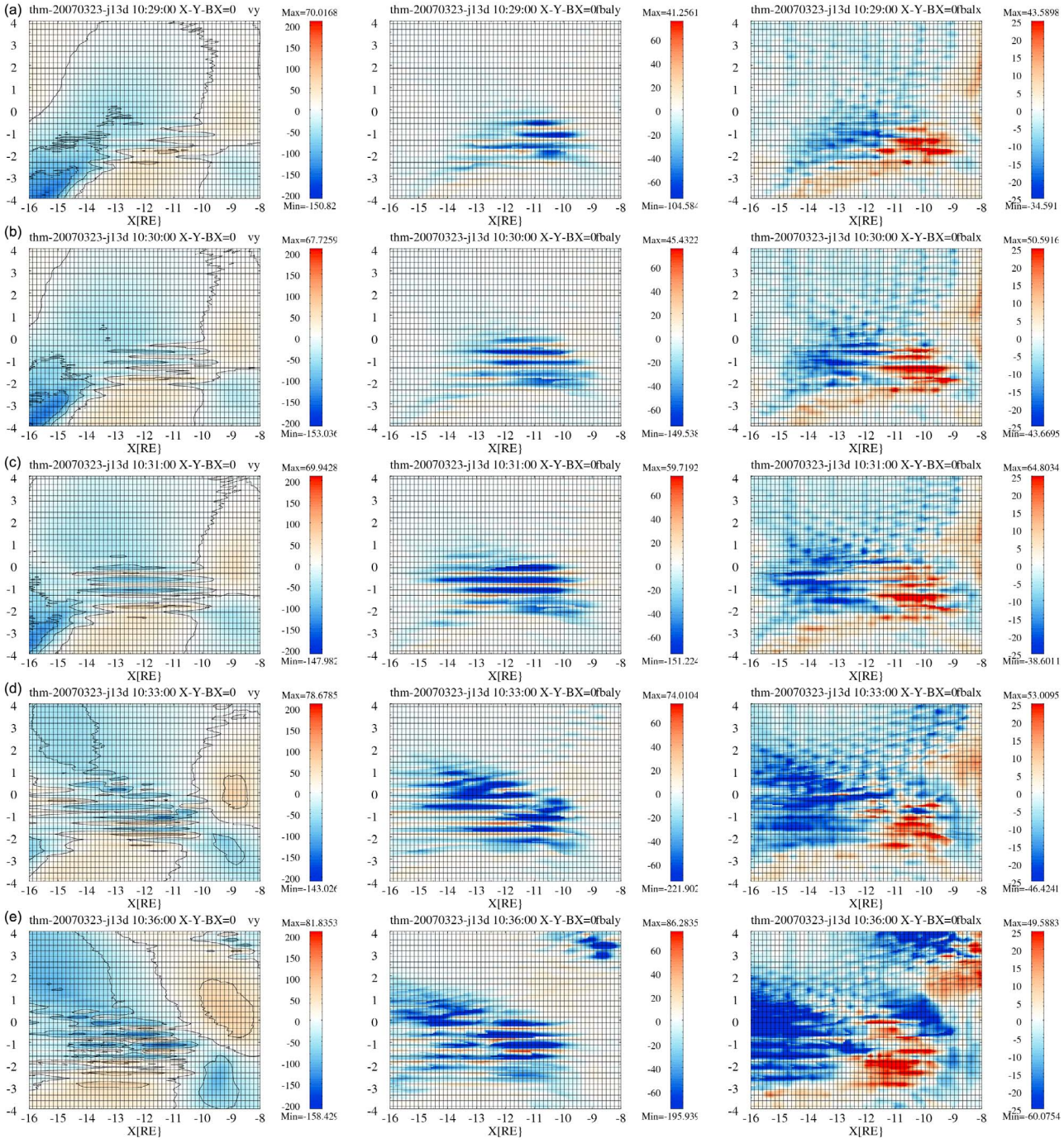

Figure 4. Variables in the center of the current sheet, in the same format as in Figure 3. The (left) V_y, (middle) force balance in the y direction($\tilde{F}_y = (\mathbf{j} \times \mathbf{B} - \nabla \mathbf{p})_y$), and (right) force balance in the x direction, $\tilde{F}_x$, are shown.

shows strong tailward flows with superimposed reductions of tailward flow. Consistent with V_x, the force imbalance $\tilde{F}_x$ (Figure 4, right) is also predominantly tailward, as we previously concluded. Thus, the instability observed here is not a pure ballooning mode as discussed in the literature. It appears that the ballooning mode is superimposed on a different mode that has no significant y dependence. The existence of such a mode, which stretches across the entire plasma sheet is also more consistent with the subsequent development of the tearing mode. The ballooning mode, by itself, would create small channels in which the flow accelerates tailward, and thus has a positive divergence. The positive divergence reduces the B_z field component in the current sheet, according to Faraday's law in ideal MHD

$$\frac{\partial \mathbf{B}}{\partial t} = \nabla \times (\mathbf{v} \times \mathbf{B}), \tag{11}$$

which can be rewritten appropriate for conditions in the current sheet considering only B_z, assuming that B_x and B_y are zero, and that there is only variation in x, as

$$\frac{\partial B_z}{\partial t} = -v_x \frac{\partial B_z}{\partial x} - B_z \frac{\partial v_x}{\partial x} \Rightarrow \frac{dB_z}{dt} = -B_z \frac{\partial v_x}{\partial x}. \quad (12)$$

[32] Thus the flow transports magnetic flux tailward, and at the same time the positive divergence of the flow reduces B_z. This is also evident in Figure 2e, which shows that starting at T~212 min and x~−14 R_E B_z significantly decreases, just where the flow divergence is strongest, as seen in Figure 2a. The reduction of B_z then paves the way for the tearing mode to grow, which is otherwise stabilized by the normal field [*Somov and Verneta*, 1993; *Harrold et al.*, 1995]. If there was only the large k_y ballooning mode present, there should be fingers of reduced B_z alternating with fingers of increased B_z. The tearing mode should in that case only grow in the small channels with reduced B_z, but this is not what we observe in the simulation. The existence of the k_y ~0 mode thus seems necessary to initiate reconnection in a wide (several R_E) section of the tail, which is required for the substorm to commence. In the following, we will call this mode the "KY0" mode to distinguish it from the ballooning mode with large k_y.

[33] Next, we address whether or not the ballooning mode is sufficiently resolved in this simulation. Figure 5 shows results from a simulation of the same event with increased resolution in the y coordinate. Specifically, in this simulation Δy = 0.16 R_E (~1000 km) versus Δy = 0.25 R_E (~1600 km) in the previous one. For this simulation we show the results for the variables V_y, $\tilde{F}_y$, and $\tilde{F}_x$, and for the times 1029 UT, 1036 UT, and 1040 UT, which is sufficient to make our point. Because the substorm onset occurs somewhat later in this simulation, we added the 1040 UT time. The finger structures are now clearly resolved. Moreover, most of them are no longer aligned with the grid, but are oriented at various angles to the grid lines. This is most evident in the $\tilde{F}_y$ plot at 1040 UT, i.e., Figure 5c (middle). The wavelength is essentially the same as in the previous simulation, i.e., of the order of 0.5 R_E. This wavelength is fully consistent with recent Geotail observations [*Saito et al.*, 2008] which also showed ballooning oscillations with a wavelength of ~3000 km. It is not clear at this point what determines that wavelength. Theoretical studies usually assume that kinetic effects are responsible for setting the characteristic length scale [*Vetoulis and Chen*, 1994; *Bhattacharjee et al.*, 1998; *Cheng and Zaharia*, 2004], yet in our simulations it must be a MHD effect, which is possibly affected by physical and numerical dissipation. However, investigating this question, and others related to the ballooning mode in our simulations, are beyond the scope of this paper and will be addressed separately.

[34] Lastly, we address the growth rate of the instability. Figure 6 shows the time evolution of various quantities at the center of the plasma sheet. The variables are plotted on a logarithmic scale to better exhibit the exponential growth phases and saturation. All time series are taken in the Y = 0 meridian and at X_{GSE} = −15 R_E, but similar results are obtained at other locations where the instabilities grow.

[35] The most dramatic growth is observed in V_x. It grows by more than a factor 20, starting at T = 208 min, to T~211 min, i.e., within 3 minutes. There is a further increase of V_x after T = 211 min, but that is clearly associated with reconnection. This growth time is remarkably consistent with recent observation of low-latitude auroral arcs that grow exponentially in luminosity for ~2–4 min before the auroral substorm breakup [*Donovan et al.*, 2008; *Liang et al.*, 2008]. Although we cannot at present establish the physical connection between such arcs and the instability that we find in our simulation, it is certainly worth exploring the existence of such a link. The connection may be tenuous, though, because the observed arcs are much less bright than typical arcs during the expansion phase.

[36] The parallel electric field $E_{||}$ begins to grow with a slight delay after V_x, and it also grows by almost a factor of 20. The temperature roughly follows the time development of $E_{||}$; however, the overall temperature increase is much smaller.

[37] The growth of the current density, i.e., the thinning of the current sheet, and the decrease of B_z in the current sheet occur simultaneously and on a faster time scale, ~2 minutes. This time scale is somewhat longer, but still consistent with time scale of the "explosive growth phase" (~1 min) postulated by *Ohtani et al.* [1992].

[38] At T~212 min there is a discontinuity in the slope of nearly all variables. The growth rate of V_x slows, $E_{||}$ reaches a local maximum, the growth of the current density slows, and B_z reaches a minimum. As previously shown, this marks the onset of reconnection.

5. Summary and Discussion

[39] We have presented a detailed analysis of an OpenGGCM simulation run of the 23 March 2007 substorm. This substorm has previously been studied by several authors [*Angelopoulos et al.*, 2008a; *Runov et al.*, 2008; *Raeder et al.*, 2008; *Zhu et al.*, 2009]. In particular, *Raeder et al.* [2008] and *Zhu et al.* [2009] have used OpenGGCM simulations to study this substorm. The former study did not address the specific substorm onset mechanism, whereas the latter study applied ballooning stability criteria to examine if the tail could possibly be unstable to ballooning. Indeed, *Zhu et al.* [2009] found that the criteria for ballooning were at times fulfilled. However, conventional wisdom predicted that the ballooning mode could only exist at large k_y and thus it could not be resolved by a global simulation. Therefore, no search for the signatures of the ballooning mode was performed. Likewise, this study did not aim at finding ballooning signatures, but its goal was to investigate the instability that precedes the formation of a new near-Earth x line. The "discovery" of the ballooning structures was purely serendipitous. Thus, we are able to present in this paper not only a new scenario for substorm onset, but also the first simulation of ballooning modes in the geomagnetic tail in a global code.

[40] The analysis of the simulation run shows that the growth phase seamlessly transitions into two ideal instabilities in the near Earth tail. This transition seems to be at the heart of the 2 min problem [*Angelopoulos et al.*, 2008b, 2009; *Lui*, 2009], i.e., the sequence of physical processes that leads to the substorm expansion phase. Any distinction whether this

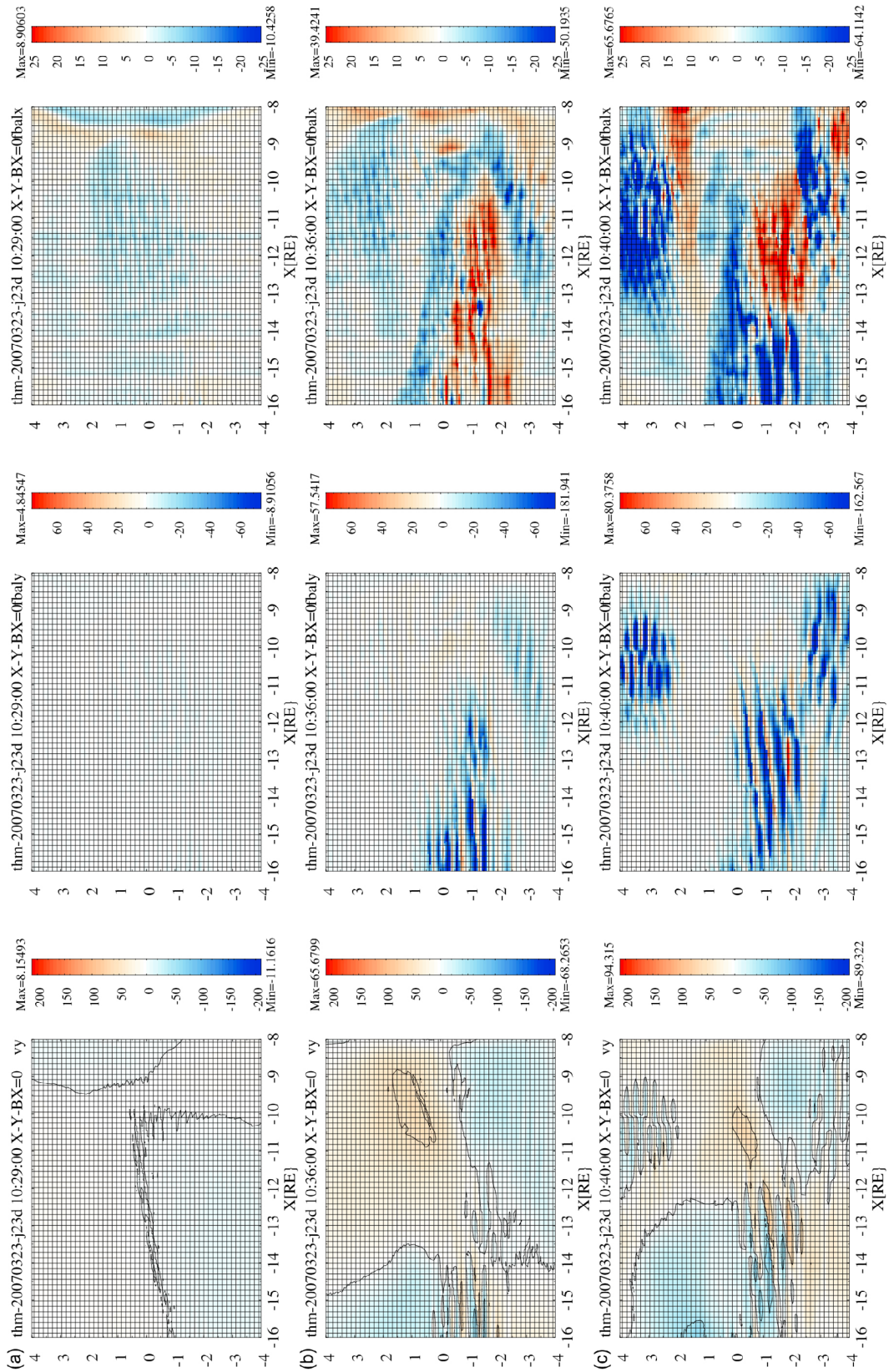

Figure 5. Variables in the center of the current sheet, in the same format as in Figures 3 and 4, but for a simulation run with higher resolution in the y direction. The (left) V_y, (middle) force balance in the y direction ($\tilde{F}_y = (\mathbf{j} \times \mathbf{B} - \nabla \mathbf{p})_y$), and (right) force balance in the x direction, $\tilde{F}_x$, are shown. Since the substorm evolves somewhat different in this simulation, the times (a) 1029 UT, (b) 1036 UT, and (c) 1040 UT are shown.

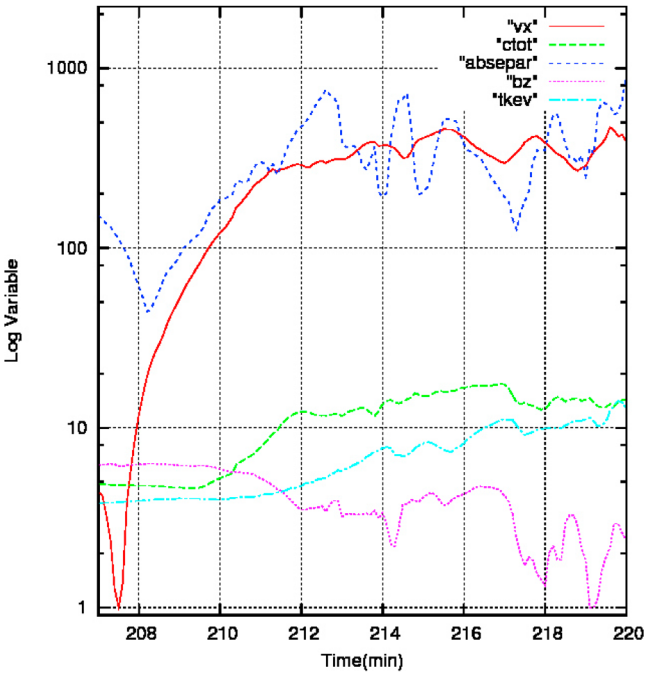

Figure 6. Time series at the center of the current sheet, Y = 0, and X = −15R_E. Here "vx" is the negative of the x component of the velocity in km/s, "bz" is B_z in nT, "absepar" is $E_{\|}$ in μV/m, and "ctot" is the current density in nA/m^2.

instability is still part of the growth phase or already part of the expansion phase would be purely semantic. We thus stay with the current nomenclature and call it the explosive growth phase (EGP). As shown here, the EGP is made up of two instabilities. One is the well-known ballooning mode, which has been extensively studied in the literature. Our simulation by and large confirms the theoretical predictions. The ballooning mode appears exactly where it was predicted by *Zhu et al.* [2009], who used exactly the same simulation run that has been analyzed in this paper. The wavelength of the ballooning mode is found to be of the order of 0.5 R_E, which is also consistent with recent observations [*Saito et al.*, 2008]. It is not clear, however, what determines the spatial scale. Since kinetic effects are not included in the simulation MHD processes must control the scale.

[41] The second instability, the KY0 mode, is new and was not known prior to the discovery by *Siscoe et al.* [2009], who speculated that it may have common features, and possibly the same physical mechanism, as those responsible for coronal mass ejections. How the ballooning mode and the KY0 mode are related is not clear. In our simulation they appear to occur at the same time and the same locations. However, we cannot rule out that one precedes the other or that they begin to grow in separate spatial regions and only later overlap. More detailed analysis and more simulation runs, in particular with higher resolution, are required to answer this question. A better theoretical understanding of the KY0 mode would also be helpful.

[42] Our simulations suggest a new phenomenological model for the onset of the substorm expansion phase. During the growth phase the tail undergoes a slow evolution by which magnetic flux and energy is added to the lobes, and the plasma sheet and current sheet become thinner. There are no substantial flows, i.e., this evolution is quasi static and can be described by a sequence of equilibria. Such equilibria have been modeled extensively. As this evolution progresses a point is reached at which an equilibrium is no longer possible. At this point the KY0 mode and the ballooning mode begin to grow. Their evolution is exponential, which is typical for instabilities in their linear phase. These ideal MHD modes lead to accelerating tailward flows. The divergence of this flow reduces the B_z component in the current sheet. This reduces the averaged (over the thickness of the current sheet) $\mathbf{j} \times \mathbf{B}$ force, because the averaged j_y remains roughly constant, as sown in equation (4). One can write out an evolution equation as equation (12) for the pressure. Thus the pressure distribution along the tail axis becomes stretched out and flattened, reducing the tailward pressure gradient force as well. As already shown by *Siscoe et al.* [2009] the $\mathbf{j} \times \mathbf{B}$ force is reduced more, and thus the KY0 instability ensues. The question why the force imbalance occurs is still open and will be addressed in a separate paper.

[43] Since finite B_z in the current sheet has a strong stabilizing effect on the tearing mode (it makes it difficult to change the magnetic topology and form a new x line), the current sheet remains tearing stable until the B_z is sufficiently reduced. At that point, the tearing mode begins to grow and quickly overtakes the other instabilities. The finger like structures of the classical ballooning mode are still present well after the tearing mode has commenced; however, their role in the dynamics is unclear. We speculate that the ballooning and KY0 modes may have visible auroral counterparts, possibly driven by changes in the near-Earth pressure distribution. However, the auroral breakup and WTS require much more energy than the ideal MHD modes can release and are thus likely driven by the subsequent reconnection.

[44] Still, many questions remain open. First, and foremost, it is not clear whether this scenario is ubiquitous or only applies to some substorms. Of course, there may also be important kinetic effects that are not included in the MHD description. The connection between the tail processes and auroral and ionospheric features still needs to be explored. Although most of the signatures predicted by the model have been observed, one way or the other, a full experimental confirmation will require the observation of the entire sequence of events with proper spatial and temporal coverage. Such observations will likely have to wait until a constellation mission with 10s or 100s of satellites covers a good part of the nightside plasma sheet.

[45] **Acknowledgments.** This research was supported by NASA grant NAS5-02099 (THEMIS) and NSF grants ATM-0639658 and ATM-0902360. Development of the OpenGGCM has been supported by NASA grant NNG05GM57G and NSF grant ATM-0639658. G.S. was in part supported by NSF grant ATM-0809307. Part of the simulations were performed at the National Center for Supercomputer Applications (NCSA). Part of this work was accomplished while J.R. was on sabbatical at CESR, Toulouse, France. He would like to thank the CESR staff, and Benoit Lavraud in particular, for their hospitality and support.

[46] Bob Lysak thanks the reviewers for their assistance in evaluating this paper.

References

Angelopoulos, V., et al. (2008a), First results from the THEMIS mission, *Space Sci. Rev.*, *141*, 453.

Angelopoulos, V., et al. (2008b), Tail reconnection triggering substorm onset, *Science*, *321*, 931.
Angelopoulos, V., J. McFadden, D. Larson, C. W. Carlson, S. Mende, and H. Frey (2009), Response to comment on "Tail reconnection triggering substorm onset," *Science*, *324*, 1391.
Baker, D. N., T. I. Pulkkinen, V. Angelopoulos, W. Baumjohann, and R. L. McPherron (1996), Neutral line model of substorms: Past results and present view, *J. Geophys. Res.*, *101*, 12,975.
Baker, D. N., T. I. Pulkkinen, J. Buchner, and A. J. Klimas (1999), Substorms: A global instability of the magnetosphere-ionosphere system, *J. Geophys. Res.*, *104*, 14,601.
Bhattacharjee, A., Z. W. Ma, and X. Wang (1998), Dynamics of thin current sheets and their disruption by ballooning instabilities: A mechanism for magnetospheric substorms, *Phys. Plasmas*, *5*, 2001, doi:10.1063/1.872871.
Birn, J. (1987), Magnetotail equilibrium theory: The general three-dimensional solution, *J. Geophys. Res.*, *92*, 11,101.
Birn, J., and M. Hesse (1992), Influence of plasma sheet thickening towards the tail flanks on magnetotail stability and dynamics, *J. Geophys. Res.*, *99*, 5847.
Birn, J., and K. Schindler (2002), Thin current sheets in the magnetotail and the loss of equilibrium, *J. Geophys. Res.*, *107*(A7), 1117, doi:10.1029/2001JA000291.
Birn, J., J. Raeder, Y. L. Wang, R. A. Wolf, and M. Hesse (2004), On the propagation of bubbles in the geomagnetic tail, *Ann. Geophys.*, *22*, 1773.
Chen, C. X., and R. A. Wolf (1993), Interpretation of high speed flows in the plasma sheet, *J. Geophys. Res.*, *98*, 12,939.
Chen, C. X., and R. A. Wolf (1999), Theory of thin-filament motion in Earth's magnetotail and its application to bursty bulk flows, *J. Geophys. Res.*, *104*, 14,613.
Cheng, C. Z., and S. Zaharia (2004), MHD ballooning instability in the plasma sheet, *Geophys. Res. Lett.*, *31*, L06809, doi:10.1029/2003GL018823.
Coroniti, F. V., and C. F. Kennel (1972), Changes in magnetospheric configuration during the substorm growth phase, *J. Geophys. Res.*, *77*, 3361.
Donovan, E., et al. (2008), Simultaneous THEMIS in situ and auroral observations of a small substorm, *Geophys. Res. Lett.*, *35*, L17S18, doi:10.1029/2008GL033794.
Elsen, R. K., R. M. Winglee, J. F. Spann, G. A. Germany, M. Brittnacher, and G. K. Parks (1998), The auroral oval boundaries on January 10, 1997: A comparison of global magnetospheric simulations with UVI images, *Geophys. Res. Lett.*, *25*, 2585.
Evans, C. R., and J. F. Hawley (1988), Simulation of magnetohydrodynamic flows: A constrained transport method, *Astrophys. J.*, *332*, 659.
Fuller-Rowell, T. J., D. Rees, S. Quegan, R. J. Moffett, M. V. Codrescu, and G. H. Millward (1996), A coupled thermosphere-ionosphere model (CTIM), in *STEP Report*, edited by R. W. Schunk, pp. 217–238, Sci. Comm. on Sol. Terr. Phys., Natl. Geophys. Data Cent., NOAA, Boulder, Colo.
Gabrielse, C., et al. (2009), Timing and localization of near-Earth tail and ionospheric signatures during a substorm onset, *J. Geophys. Res.*, *114*, A00C13, doi: 10.1029/2008JA013583. [Printed *115*(A1), 2010.]
Harrold, B. G., A. Bhattacharjee, and X. Wang (1995), Tearing stability of the two-dimensional magnetotail, *Phys. Plasmas*, *2*, 3857.
Hesse, M., and J. Birn (1993), Three-dimensional magnetotail equilibria by numerical relaxation techniques, *J. Geophys. Res.*, *98*, 3973.
Hesse, M., T. G. Forbes, and J. Birn (2005), On the relation between reconnected magnetic flux and parallel electric fields in the solar corona, *Astrophys. J.*, *631*, 1227.
Hones, E. W. (1979), Transient phenomena in the magnetotail and their relation to substorms, *Space Sci. Rev.*, *23*, 393.
Hu, B., F. R. Toffoletto, R. A. Wolf, S. Sazykin, J. Raeder, D. Larson, and A. Vapirev (2010), One-way coupled OpenGGCM/RCM simulation of the 23 March 2007 substorm event, *J. Geophys. Res.*, *115*, A12205, doi:10.1029/2010JA015360.
Kepko, L., M. G. Kivelson, and R. L. McPherron (2004), Relative timing of substorm onset phenomena, *J. Geophys. Res.*, *109*, A04203, doi:10.1029/2003JA010285.
Kuznetsova, M. M., M. Hesse, L. Rastätter, A. Taktakishvili, G. Toth, D. L. D. Zeeuw, A. Ridley, and T. I. Gombosi (2007), Multiscale modeling of magnetospheric reconnection, *J. Geophys. Res.*, *112*, A10210, doi:10.1029/2007JA012316.
Lee, D. Y., and R. A. Wolf (1992), Is the Earth's magnetotail balloon unstable?, *J. Geophys. Res.*, *97*, 19,251.
Lemon, C. (2004), Magnetic storm ring current injection modeled with the Rice Convection Model and a self-consistent magnetic field, *Geophys. Res. Lett.*, *31*, L21801, doi:10.1029/2004GL020914.
Liang, J., E. F. Donovan, W. W. Liu, B. Jackel, M. Syrjäsuo, S. B. Mende, H. U. Frey, V. Angelopoulos, and M. Connors (2008), Intensification of preexisting auroral arc at substorm expansion phase onset: Wave-like disruption during the first tens of seconds, *Geophys. Res. Lett.*, *35*, L17S19, doi:10.1029/2008GL033666.
Liou, K., C.-I. Meng, A. T. Y. Lui, P. T. Newell, and S. Wing (2002), Magnetic dipolarization with substorm expansion onset, *J. Geophys. Res.*, *107*(A7), 1131, doi:10.1029/2001JA000179.
Lui, A. T. Y. (2009), Comment on "Tail reconnection triggering substorm onset," *Science*, *324*, 1391.
Lui, A. T. Y., et al. (1992), Current disruptions in the near-Earth neutral sheet region, *J. Geophys. Res.*, *97*, 1461.
Lui, A. T. Y., et al. (2007), Prelude to THEMIS tail conjunction study, *Ann. Geophys.*, *25*, 1001.
Lyon, J. G., S. H. Brecht, J. A. Fedder, and P. J. Palmadesso (1981), Computer simulation of a geomagnetic substorm, *Phys. Rev. Lett.*, *46*, 1038.
McPherron, R. L. (1972), Substorm related changes in the geomagnetic tail: the growth phase, *Planet. Space Sci.*, *20*, 1521.
McPherron, R. L., (1991), Physical processes producing magnetospheric substorms and magnetic storms, in *Geomagnetism*, vol. 4, edited by J. Jacobs, pp. 593–739, Academic, London.
Mende, S. B., S. E. Harris, H. U. Frey, V. Angelopoulos, C. T. Russell, E. Donovan, B. Jackel, M. Greffen, and L. M. Peticolas (2009), The THEMIS array of ground-based observatories for the study of auroral substorms, *Space Sci. Rev.*, *141*, 357.
Ohtani, S. I., and T. Tamao (1993), Does the ballooning instability trigger substorms in the near-Earth magnetotail?, *J. Geophys. Res.*, *98*, 19,369.
Ohtani, S., K. Takahashi, L. Zanetti, T. Potemra, R. McEntire, and T. Iijima (1992), Initial signatures of magnetic field and energetic particle fluxes at tail reconfiguration: Explosive growth phase, *J. Geophys. Res.*, *97*, 19,311.
Pu, Z. Y., A. Korth, Z. X. Chen, Z. X. Liu, S. Y. Fu, G. Zong, M. H. Hong, and X. M. Wang (2001), A global synthesis model of dipolarization at substorm expansion onset, *J. Atmos. Sol. Terr. Phys.*, *63*, 671.
Pulkkinen, T. I., D. N. Baker, M. Wiltberger, C. Goodrich, R. E. Lopez, and J. G. Lyon (1998), Pseudobreakup and substorm onset: Observations and MHD simulations compared, *J. Geophys. Res.*, *103*, 14,847.
Rae, I. J., et al. (2009), Timing and localization of ionospheric signatures associated with substorm expansion phase onset, *J. Geophys. Res.*, *114*, A00C09, doi:10.1029/2008JA013559. [Printed *115*(A1), 2010.]
Raeder, J. (1995), Global MHD simulations of the dynamics of the magnetosphere: Weak and strong solar wind forcing, in *Proceedings of the Second International Conference on Substorms*, edited by J. R. Kan, J. D. Craven, and S.-I. Akasofu, pp. 561–568, Geophys. Inst., Univ. of Alaska Fairbanks, Fairbanks, Alaska.
Raeder, J. (2003), Global magnetohydrodynamics—A tutorial, in *Space Plasma Simulation*, edited by J. Büchner, C. T. Dum, and M. Scholer, pp. 212–246, Springer, Berlin.
Raeder, J., and N. Maynard (2001), Foreword, *J. Geophys. Res.*, *106*, 345.
Raeder, J., and R. L. McPherron (1998), Global MHD simulations of the substorm current wedge and dipolarization, in *Substorms-4*, edited by S. Kokubun and Y. Kamide, pp. 343–348, Kluwer Acad., Dordrecht, Netherlands.
Raeder, J., et al. (2001a), Global simulation of the geospace environment modeling substorm challenge event, *J. Geophys. Res.*, *106*, 381.
Raeder, J., Y. L. Wang, and T. Fuller-Rowell (2001b), Geomagnetic storm simulation with a coupled magnetosphere-ionosphere-thermosphere model, in *Space Weather*, *Geophys. Monogr. Ser.*, vol. 125, edited by P. Song, G. Siscoe, and H. J. Singer, pp. 377–384, AGU, Washington, D. C.
Raeder, J., D. Larson, W. Li, E. L. Kepko, and T. Fuller-Rowell (2008), OpenGGCM simulations for the THEMIS mission, *Space Sci. Rev.*, *141*, 535, doi:10.1007/s11214-008-9421-5.
Roux, A., et al. (1991), Plasma sheet instability related to the westward traveling surge, *J. Geophys. Res.*, *96*, 17,714.
Runov, A., V. Angelopoulos, N. Ganushkina, R. Nakamura, J. McFadden, D. Larson, I. Dandouras, K. H. Glassmeier, and C. Carr (2008), Multipoint observations of the inner boundary of the plasma sheet during geomagnetic disturbances, *Geophys. Res. Lett.*, *35*, L17S23, doi:10.1029/2008GL033982.
Russell, C. T., and R. L. McPherron (1973), The magnetotail and substorms, *Space Sci. Rev.*, *15*, 205.
Saito, M., Y. Miyashita, M. Fujimoto, I. Shinohara, Y. Saito, K. Liou, and T. Mukai (2008), Ballooning mode waves prior to substorm-associated dipolarizations: Geotail observations, *Geophys. Res. Lett.*, *35*, L07103, doi:10.1029/2008GL033269.
Sazykin, S., R. A. Wolf, R. W. Spiro, T. I. Gombosi, D. L. DeZeeuw, and M. F. Thomsen (2002), Interchange instability in the inner magnetosphere associated with geosynchronous particle flux decreases, *Geophys. Res. Lett.*, *29*(10), 1448, doi:10.1029/2001GL014416.

Sergeev, V. A., P. Tanskanen, K. Mursula, A. Korth, and R. C. Elphic (1990), Current sheet thickness in the near-Earth plasma sheet during substorm growth phase, *J. Geophys. Res.*, *95*, 3819.

Sibeck, D. G., and V. Angelopoulos (2008), THEMIS science objectives and mission phases, *Space Sci. Rev.*, *141*, 35.

Siscoe, G. L., M. M. Kuznetsova, and J. Raeder (2009), Search for an onset mechanism that operates for both CMEs and substorms, *Ann. Geophys.*, *27*, 3141.

Slinker, S. P., J. A. Fedder, and J. G. Lyon (1995), Plasmoid formation and evolution in a numerical simulation of a substorm, *Geophys. Res. Lett.*, *22*, 859.

Somov, B. V., and A. I. Verneta (1993), Tearing instability of reconnecting current sheets in space plasmas, *Space Sci. Rev.*, *65*, 253.

Sonnerup, B. U. Ö., and M. J. Laird (1963), On the magnetospheric interchange instability, *J. Geophys. Res.*, *68*, 131.

Vetoulis, G., and L. Chen (1994), Global structures of Alfvén-ballooning modes in magnetospheric plasmas, *Geophys. Res. Lett.*, *21*, 2091.

Wiltberger, M., T. I. Pulkkinen, J. G. Lyon, and C. C. Goodrich (2000), MHD simulation of the magnetotail during the December 10, 1996, substorm, *J. Geophys. Res.*, *105*, 27,649.

Zaharia, S., and C. Z. Cheng (2003), Near-Earth thin current sheets and Birkeland currents during substorm growth phase, *Geophys. Res. Lett.*, *30*(17), 1883, doi:10.1029/2003GL017456.

Zhu, P., A. Bhattacharjee, and Z. Ma (2004), Finite k_y ballooning instability in the near-Earth magnetotail, *J. Geophys. Res.*, *109*, A11211, doi:10.1029/2004JA010505.

Zhu, P., C. R. Sovinec, C. C. Hegna, A. Bhattacharjee, and K. Germaschewski (2007), Nonlinear ballooning instability in the near-Earth magnetotail: Growth, structure, and possible role in substorms, *J. Geophys. Res.*, *112*, A06222, doi:10.1029/2006JA011991.

Zhu, P., J. Raeder, K. Germaschewski, and C. C. Hegna (2009), Initiation of ballooning instability in the near-Earth plasma sheet prior to the 23 March 2007 THEMIS substorm expansion onset, *Ann. Geophys.*, *27*, 1129.

Y. Ge and J. Raeder, Space Science Center, University of New Hampshire, 8 College Rd., Durham, NH 03824, USA. (yasong.ge@gmail.com; j.raeder@unh.edu)

G. Siscoe, Center for Space Physics, Boston University, 725 Commonwealth Ave., Boston, MA 02215, USA. (siscoe@skynet.bu.edu)

P. Zhu, Department of Engineering Physics, University of Wisconsin-Madison, 1500 Engineering Dr., Madison, WI 53706, USA. (pzhu@wisc.edu)